 FDMP, vol.14, no.2, pp.87-105, 2018

# Three-Dimensional Numerical Investigation of Convective Thermal Instabilities in the Sapphire Melt for Czochralski Growth Process

**H. Azoui[1], D. Bahloul[1, *] and N. Soltani[2]**

**Abstract:** In this work we have performed a three-dimensional numerical investigation in order to find the optimal conditions for growing efficiently high quality sapphire crystals with good thermal properties. We have studied thermal instabilities near the melt-crystal interface and the convective heat transfer under the Czochralski (Cz) process. We performed 3-D CFD simulation in cylindrical coordinates and used the Fast Fourier Transform method to analyze the temperature fluctuations. We present a detailed investigation on the effects of the crystal rotation speed and the temperature distribution on thermal instabilities of sapphire melt under forced convection. Where the melt forced convection, the radiative heat transfer and the Marangoni convection, were conducted for $Al_2O_3$ melt in the Cz crucible. We have been able to determine the optimal rotation speed giving a planar crystal-melt interface where the symmetry of the flow in the crucible is conserved witch is found to be 13 rpm for the studied case. On the other hand we achieved a visualization of the temperature fluctuations just below the interface. These fluctuations give precious information about the melt -crystal interface, which plays an important role on the quality of the pulled crystal.

**Keywords:** Forced convection, thermal instabilities, heat transfer, temperature fluctuations, sapphire, crystal growth, Czochralski technique.

## 1 Introduction

The sapphire ($Al_2O_3$) is an important material because of its exceptional optical, thermal and electrical properties [Alombert-Goget, Li, Guyot et al. (2015); Fukuda (2007)]. The combination of these properties makes it ($Al_2O_3$) suitable for a wide range of product applications [Bruni (2013)]. Sapphire shaped crystals are very required in the development of modern science and technology [Duffar (2010)], and they have several medical, military and industrial applications [Duffar (2010); Chandra and Schmid (2001)]: lasers and optical systems, cellular phone glasses, optical fibers, wave guides for surgery, needles for laser therapy and medical power delivery systems [Duffar (2010)]. Czochralski (Cz) growth technique is widely used for producing sapphire oxide single crystals $Al_2O_3$ and many other

[1] PRIMALAB Laboratory, Department of Physics, University of Batna1, 1 rue Chahid Boukhlouf Mohamed El-Hadi, 05000 Batna, Algeria.
[2] LESEI Laboratory, Department of Mechanical Engineering, University of Batna 2, 53 Route de Constantine. Fésdis, 05078 Batna, Algeria.
* Corresponding Author: Derradji Bahloul1. Email: dbahloul@gmail.com.

crystals such as, YAG, $LiNbO_3$, GGG, BGO, BaBrCl-BaBrCl: Eu and LGT [Tavakoli (2014); Yan, Shalapska and Bourret (2016); Stelian, Nehari, Lasloudji et al. (2017)] which have many applications in different technologies such as lasers, nonlinear optics, and substrates [Tavakoli (2008)]. The Cz process allows the growth of larger, high optical-quality sapphire crystals with fewer defects. However, crystals grown by this method (CZ) require strict control of the flow and temperature in the melt in order to obtain high quality crystals with adequate optical and mechanical properties [Soltani and Rahal (2017)]. Indeed, temperature distribution and forced convection in the molten sapphire during the manufacturing process are pertinent factors that affect largely on different properties of the obtained sapphire crystals.

Different types of heat transfer mechanism coexist in the Cz growth setups which are free and forced convection, conduction, within the melt, conduction and radiation between the exposed surfaces [Tavakoli (2014)]. Because the quality of the grown crystal is directly related to the transport phenomena in Cz process. Several researchers studied: Detailed analyses during the growth of high melting oxide crystals of the interface shape, transition and its inversion [Xiao and Derby (1994, 1995); Wu, Geng and Guo (1996); Tavakoli and Wilke (2007)], convective heat transfer such as melt hydrodynamics [Kobayashi (1978); Derby, Atherton and Gresho (1989); Jing, Imaishi and Sato (2000)], Influence of Marangoni convection and Influence of the crucible bottom shape on the heat transfer and fluid flow can be found in reports [Gałazka and Wilke (2000); Tavakoli and Wilke (2007).] respectively, flow transitions and instabilities in simulated Czochralski method [Brandle (1982); Kimura (1986); Kimura (1986)].

3-D numerical investigation of convective thermal instabilities and fluctuations in the sapphire melt for Cz growth process is presented in this paper. The goal of this research is to determine the optimal rotation speed giving a planar crystal-melt interface where the symmetry of the flow in the crucible is conserved. This condition plays an important role on the quality of the pulled crystal. On the other hand we achieved a visualization of the temperature fluctuations just below the interface in the case of a rotating seed. In this work we have performed a numerical simulation of the growing process with the Cz technique. The theoretical analysis of this method for the growth of sapphire single crystals is conducted using the mass, momentum, and energy conservation laws. We have used a model based on the finite volume method and analyzed the temperature fluctuations with the Fast Fourier Transform method. This model has been previously used by W. Soltani and S. Rahal to study the growth of Silicone Oil using the CZ process [Soltani and Rahal (2017)] and validated experimentally by comparing their results with those obtained by Rahal et al. [ Rahal , Cerisier and Azuma (2008)].

In the next section we present the modeled growth system. In Section 3 we have explained our assumptions, mathematical formulation of our model that is the governing equations, the boundary conditions used in our simulations. Section 4 is devoted to the results and discussion, followed by conclusion in Section 5.

## 2 Apparatus of Czochralski growth system

The Czochralski crystal growth furnace is schematically illustrated in Fig. 1. In this process, the melt is placed in a cylindrical crucible, located in a furnace. It is heated above the melting

temperature of sapphire by a radiofrequency inductive heating system [Tavakoli (2014); Tavakoli and Wilke (2007)]. A cylindrical crystal grows due to the phase change phenomena occurring at the crystal-melt interface [Soltani and Rahal (2017)]. The rotating crystal produced is vertically pulled out of the melt as shown in Fig. 1.

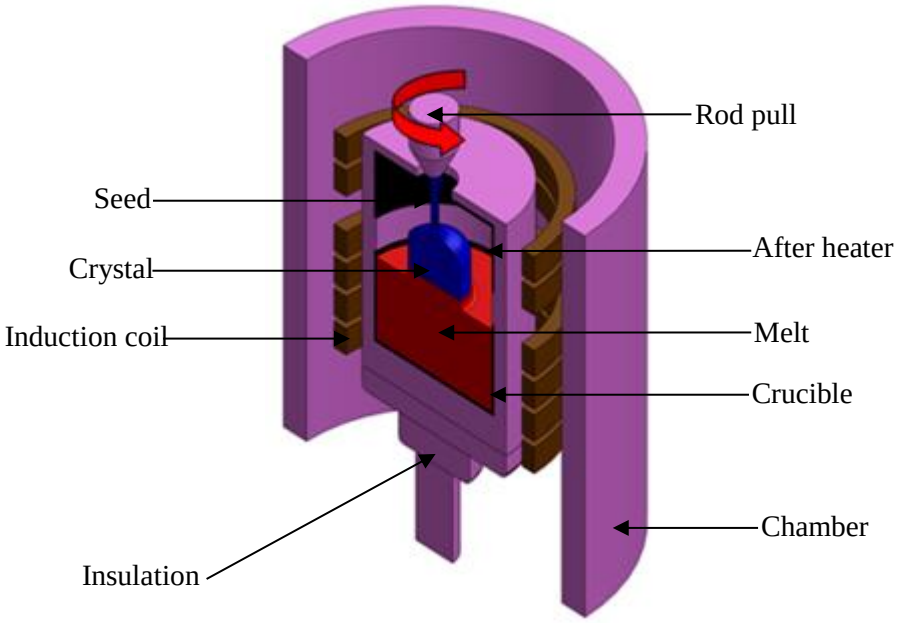


**Figure 1:** Schematization of the inductively heated Czochralski furnace

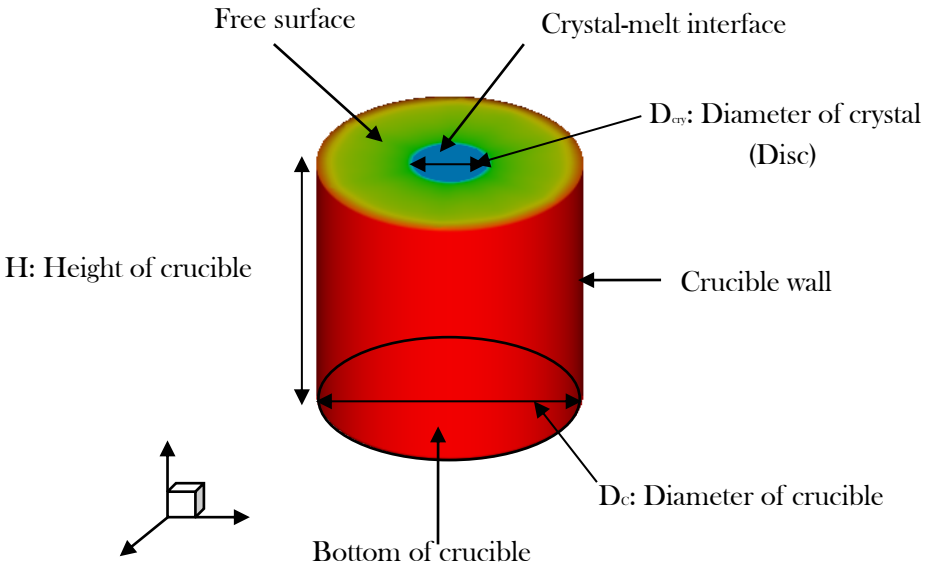


**Figure 2:** Schematic diagram of the Czochralski crucible

Fig. 2 shows the crucible geometry which depends on the used Czochralski technique. Where, $H = 0.1$ m is the crucible height and $R_c = 0.05$ m its radius. The interface melt/crystal has a diameter of $D_{cry} = 0.03$ m and a radius $R_{cry} = 0.015$ m . In the figure below, the red color presents the melt sapphire in the crucible and the blue color presents the interface between the crystal and the melt.

Our model has been previously used by Soltani et al. [Soltani and Rahal (2017)] and it is validated experimentally by comparing their results with those obtained by Rahal et al. [Rahal, Cerisier and Azuma (2008)].

## 3 Mathematical model

The study of the problem is simplified to an incompressible flow of a Newtonian viscous fluid governed by the unsteady state Navier-Stokes equations using the Boussinesq approximation. The heat transfer in the melt is modeled by the energy equation without heat generation inside the fluid, where all the physical proprieties are independent of the temperature. We use a full three-dimensional Finite Volume model expressed in cylindrical coordinates system *(r, θ, z),* where only the melt in the crucible is studied in the case of a rotating crystal with speed $u_\theta = R_{cry}\,\omega_{cry}$; $u_r$ the radial velocity and $u_z$ the axial velocity. The rotation of the crystal is put into the model as a boundary condition at the melt-crystal interface which is considered flat. The free surface of the melt is also considered flat. The governing fundamental equations are written as follows:

Equation of radial component of the momentum:

$$\frac{\partial u_r}{\partial t}+u_r\frac{\partial u_r}{\partial r}+\frac{u_\theta}{r}\frac{\partial u_r}{\partial \theta}-\frac{u_\theta^{\,2}}{r}+u_z\frac{\partial u_r}{\partial z}= -\frac{1}{\rho_m}\frac{\partial P}{\partial r}+\nu\left(\frac{1}{r}\frac{\partial}{\partial r}\left(r\frac{\partial u_r}{\partial r}\right)-\frac{u_r}{r^2}+\frac{1}{r^2}\frac{\partial^2 u_r}{\partial \theta^2}-\frac{2}{r^2}\frac{\partial u_\theta}{\partial \theta}+\frac{\partial^2 u_r}{\partial z^2}\right)+\frac{1}{\rho_m}(\rho g_r) \tag{1}$$

Equation of azimuthally component of the momentum:

$$\frac{\partial u_\theta}{\partial t}+u_r\frac{\partial u_\theta}{\partial r}+\frac{u_\theta}{r}\frac{\partial u_\theta}{\partial \theta}-\frac{u_r u_\theta}{r}+u_z\frac{\partial u_\theta}{\partial z}= -\frac{1}{\rho_m}\frac{1}{r}\frac{\partial P}{\partial \theta}+\nu\left(\frac{1}{r}\frac{\partial}{\partial r}\left(r\frac{\partial u_\theta}{\partial r}\right)-\frac{u_\theta}{r^2}+\frac{1}{r^2}\frac{\partial^2 u_\theta}{\partial \theta^2}+\frac{2}{r^2}\frac{\partial u_r}{\partial \theta}+\frac{\partial^2 u_\theta}{\partial z^2}\right)+\frac{1}{\rho_m}(\rho g_\theta) \tag{2}$$

Equation of axial component of the momentum:

$$\frac{\partial u_z}{\partial t}+u_r\frac{\partial u_z}{\partial r}+\frac{u_\theta}{r}\frac{\partial u_z}{\partial \theta}-\frac{u_\theta^{\,2}}{r}+u_z\frac{\partial u_z}{\partial z}= -\frac{1}{\rho_m}\frac{\partial P}{\partial z}+\nu\left(\frac{1}{r}\frac{\partial}{\partial r}\left(r\frac{\partial u_z}{\partial r}\right)+\frac{1}{r^2}\frac{\partial^2 u_z}{\partial \theta^2}+\frac{\partial^2 u_z}{\partial z^2}\right)+\frac{1}{\rho_m}(\rho g_z) \tag{3}$$

Energy equation:

$$\frac{\partial T}{\partial t}+u_r\frac{\partial T}{\partial z}+\frac{u_\theta}{r}\frac{\partial T}{\partial \theta}+u_z\frac{\partial T}{\partial z}=\alpha\left[\frac{1}{r}\frac{\partial}{\partial r}\left(r\frac{\partial T}{\partial r}\right)+\frac{1}{r^2}\frac{\partial^2 T}{\partial \theta^2}+\frac{\partial^2 T}{\partial z^2}\right] \quad (4)$$

Continuity equation:

$$\frac{1}{r}\frac{\partial\left(ru_r\right)}{\partial r}+\frac{1}{r}\frac{\partial u_\theta}{\partial \theta}+\frac{\partial u_z}{\partial z}=0 \quad (5)$$

## 3.1 Presentation of the grid used

Fig. 3 shows the mesh grid which has been used to solve numerically the above equations. The physical domain is in cylindrical coordinates. It was subdivided into a number of 149000 nodes. We have checked the quality of the mesh, the maximum skewness is equal to 0.4. Around each node an elementary volume called control volume is defined. The continuity and momentum equations are discretized over this domain using the finite volume method.

All our numerical simulations were carried out using the commercial CFD software FLUENT 6.3. The SIMPLE algorithm is used to resolve the pressure-velocity coupling where the convection and diffusion terms are discredited by the second-order upwind schema.

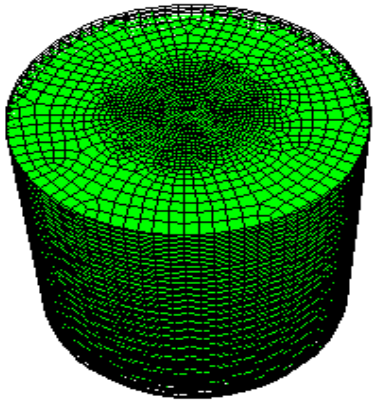

**Figure 3:** Three-dimensional mesh

### *3.2 Boundary conditions*

The cylindrical crystal is grown from the melt in a cylindrical crucible. The crystal growth model used for numerical simulation is shown in Fig. 2. In order to reduce the simulation time a disc (blue color) is used to represent the seed crystal. It is assumed that the solute is uniformly distributed in the melt reservoir. The temperature is the same at all the crucible walls. The interface shape and the melt free surface are supposed planar. The crystal-melt interface is at the melting point $T_m$. With these assumptions, we present below a description of the velocity and temperature boundary conditions used in our simulations:

-At the melt -crystal interface [Nguyen, Hsieh, Chen et al. (2016)]:

$0 \prec r \le R_{cry}, 0 \le \theta \le 2\pi, z = H$

$$T = T_m, \quad u_r = 0, \; u_\theta = R_{cry}\,\omega_{cry}, \; u_z = 0 \tag{6}$$

-At the melt free surface: $R_{cry} \le r \le R_c, 0 \le \theta \le 2\pi, z = H$

The heat transfer from the melt free surface to the ambient is controlled by both radiation and convection according to the energy balance along the melt free surface [Lan (1998)]:

$$\vec{n}.K_m \vec{\Delta T} = -Bi\left(T - T_a\right) + Rad\left(T^4 - T_a^4\right) \tag{7}$$

In this study the ambient temperature $T_a$ is set to be constant. The radiation number $Rad$ is defined by Lan [Lan (1998)]:

$$Rad = \sigma \varepsilon_m \left(R_C - R_{cry}\right) T_m{}^3 / K_m \tag{8}$$

Where σ is the Stefan Boltzmann constant, $\varepsilon_m$ is the surface emissivity of the melt and $K_m$ the thermal conductivity of the melt.

Along the free surface, the three components of the velocity are deduced from Marangoni convection; where the tangential stress balance is required:

$$\frac{\partial u_r}{\partial z} = -\frac{1}{\mu}\frac{\partial \gamma}{\partial T}\frac{\partial T}{\partial r}, \; \frac{\partial u_\theta}{\partial z} = -\frac{1}{\mu r}\frac{\partial \gamma}{\partial T}\frac{\partial T}{\partial \theta}, \; u_z = 0 \tag{9}$$

Where $\partial\gamma/\partial T$ is the surface-tension temperature coefficient and $\mu$ is the dynamic viscosity of the melt.

At the crucible side wall: $r = R_c, \; 0 \le z \le H, \; 0 \le \theta \le 2\pi$

$$\begin{aligned} T &= T_C = T_m + \Delta T \\ u_r &= 0, \; u_\theta = R_C \omega_{cry}, \; u_z = 0 \end{aligned} \tag{10}$$

At the crucible side wall, the temperature was set by the radio frequency generator. The crucible side wall temperature is about $\Delta T \approx 45$ K to 50 K above the melting point $T_m$ of sapphire [Nehari (2011)].

At the crucible bottom: $0 \le r \le R_c, \; z = 0, \; 0 \le \theta \le 2\pi$

$$T = T_C, \; u_r = 0, u_\theta = r\omega_{cry}, \; u_z = 0 \tag{11}$$

Where the crucible rotation speed $\omega_{cry}$ is taken to be null in this case. The thermo physical properties of sapphire used for our calculations are presented in Laidoune et al. [Laidoune (2010); Nehari (2011); Azoui, Laidoune, Haddad et al. (2016)] and the references therein.

## 4 Results and discussion

Since forced convection plays an important role on the quality of the grown crystal, we have achieved a comprehensive numerical study on the convective heat transfer, the profile of the temperature and temperature fluctuations inside the melt during the growth process. We have studied these different parameters in the case of the steady and unsteady state regime for different values of the crystal rotating angular speed ranging from 0 rpm up to 60 rpm.

Since the visualization of the flow characteristics in the case of sapphire are very difficult experimentally. We have compared our results in the case of another material which is studied experimentally by Rahal et al. [Rahal, Cerisier and Azuma (2008)].

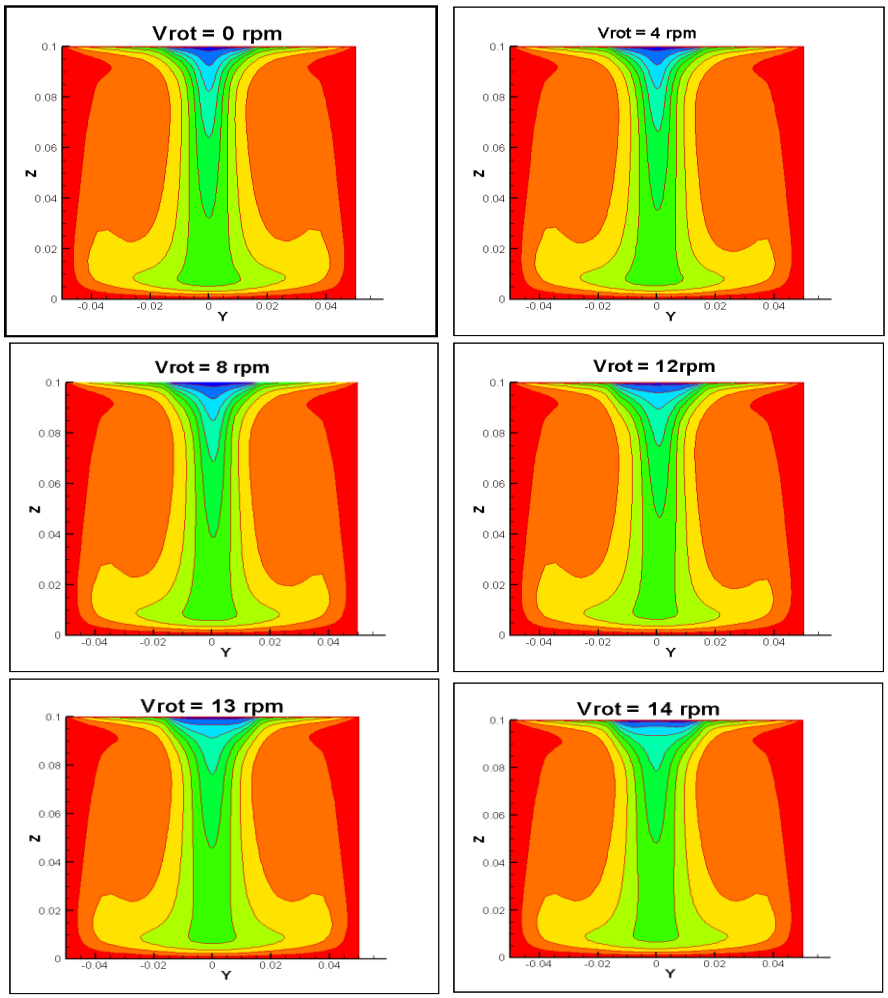

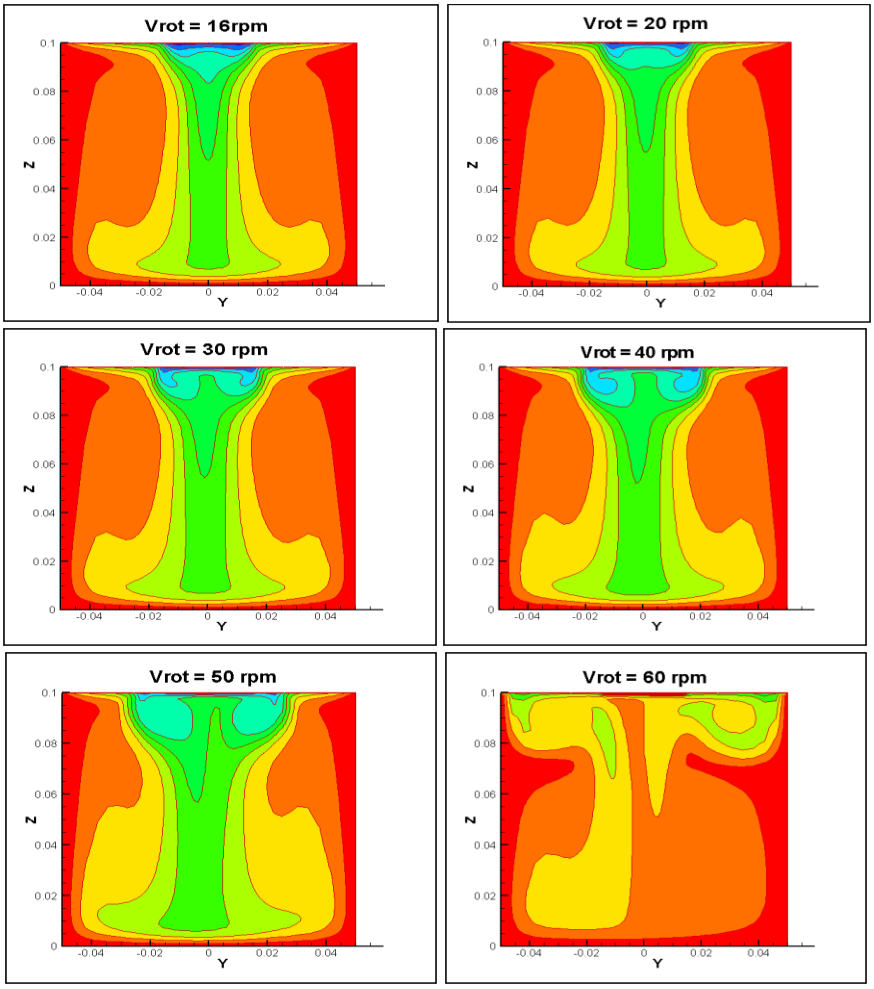


**Figure 4:** Heat transfer in the crucible's vertical median plane for sapphire melt

Fig. 4 shows the distribution of the temperature in a vertical meridian plane for $\omega_{cry} = 0 - 60$ rpm. According to these figures, we notice that starting from the crystal speed rotation $\omega_{cry} = 4$ rpm to the speed $\omega_{cry} = 30$ rpm, the temperature distribution is symmetric. This result translates the symmetry of the flow inside the crucible during the growth showing that the growth conditions are suitable for having a good quality pulled crystal. However, for $\omega_{cry} = 40$ rpm the symmetry starts to be lost and for $\omega_{cry} = 50$ rpm the temperature profile becomes totally nonsymmetrical. In this case, growth conditions are not suitable for good quality crystals. Indeed, for relatively large values of the crystal rotational speed, $\omega_{cry} \geq 40$ rpm we observe that the flow becomes nonsymmetrical in the crucible. In this case the flow becomes three-dimensional which reflects the importance of the forced convection that becomes dominant. We notice that, for a fixed Rayleigh number ( $\Delta T = 50\ K$), the heat transfer mechanism changes from a free convection regime to forced convection one when the Reynolds number increases. At

the same time we notice that the heat transfer is reinforced towards the crystal by the forced convection.

### *4.1 The radial temperature distribution in a horizontal plan*

#### *4.1.1 Unsteady state*

Fig. 5 and Fig. 6 show the radial temperature distribution in a horizontal plan 2 mm just below the crystal-melt interface in the transient (t=500 s) and steady state regime respectively.

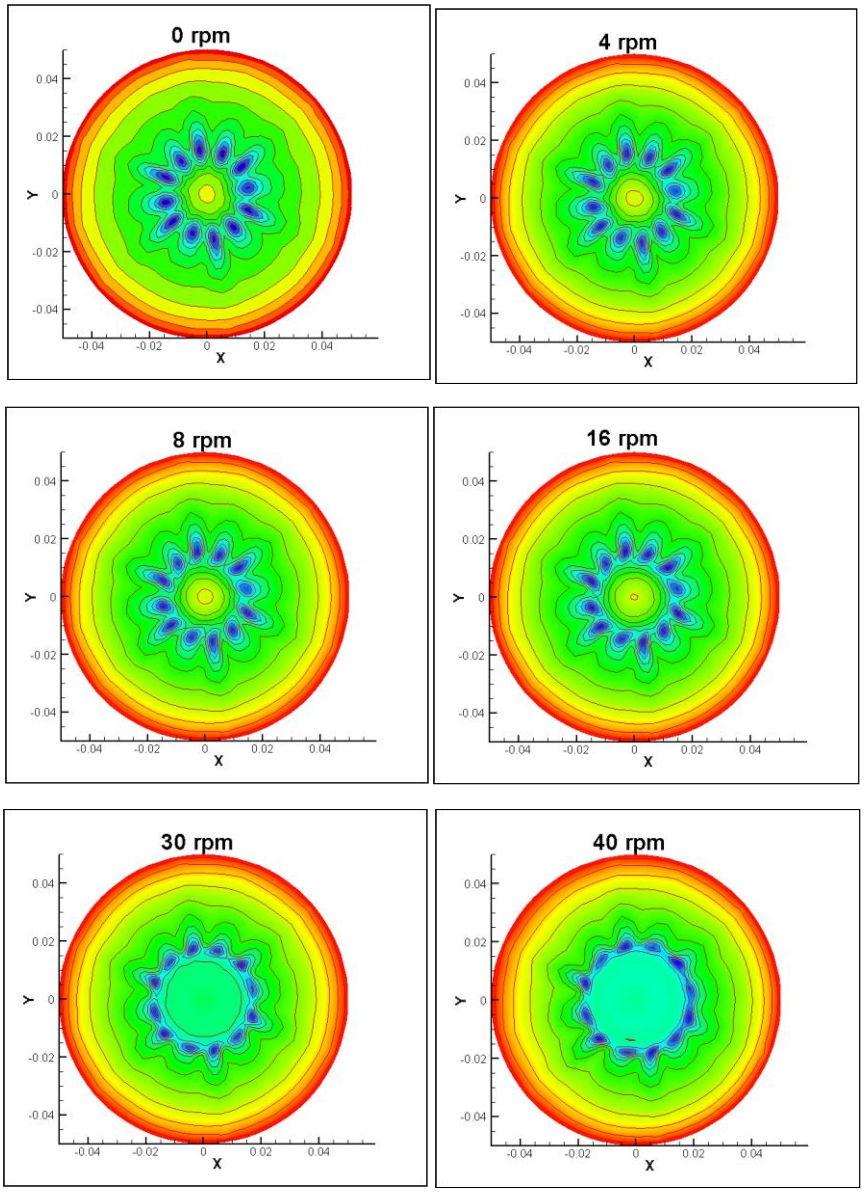

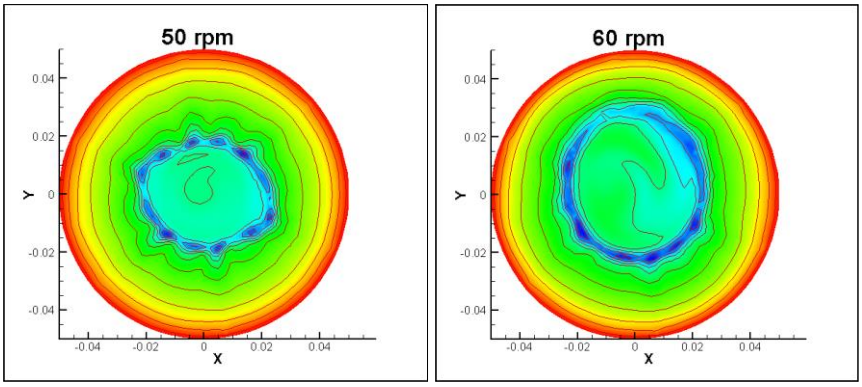


**Figure 5:** Temperature profile at a cross section (z=0.098 m) just below the melt free surface unsteady state

When the flow passes from the unsteady state to the steady state, we notice that: Near to the axis of the crystal, the fluid particles are driven by the rotational movement of the crystal. On the other hand, farther away from the crystal axis the fluid particles are less driven by the rotation of the crystal seed, leading to the formation of rotation cells which are illustrated in Fig. 5.

*4.1.2 Steady state*

When the flow approaches the steady state regime, the fluid particles along the radial distance begin to acquire the same rotation speed, which makes the rotation cells disappear. These cells give insight on the symmetry of the flow inside the crucible in the transient regime while the isothermal lines show the symmetry in the case of the steady state regime.

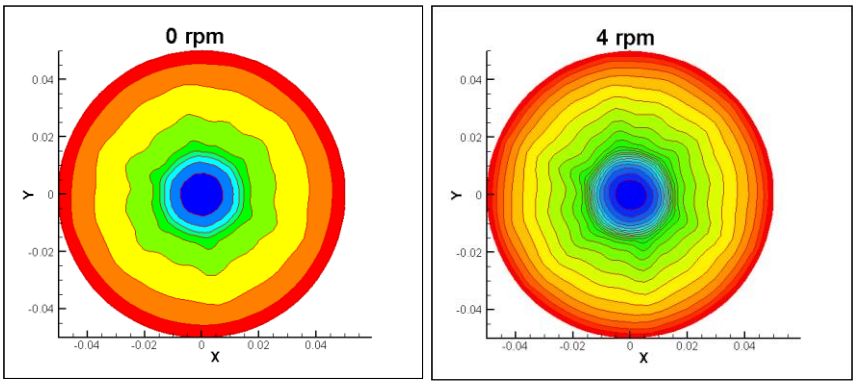

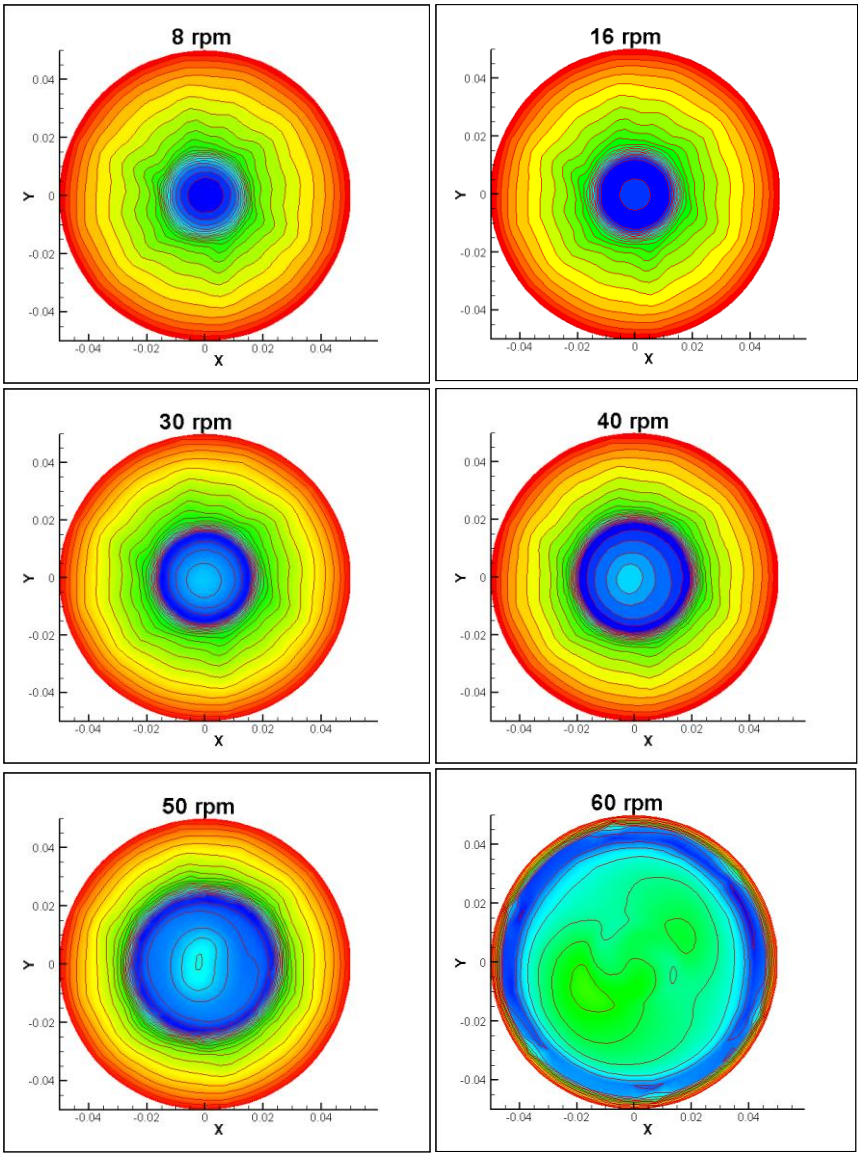


**Figure 6:** Temperature profile at a cross section (z=0.098 m) just below the melt free surface (steady state)

In both cases we notice that the flow is symmetric for relatively low rotation speeds $\omega_{cry} \leq$ 40 rpm. We notice that the symmetry starts to disappear at a rotation speed in the range $40 \leq \omega_{cry} \leq 50$ rpm. Finally, the flow becomes totally non-symmetric for $\omega_{cry} \geq$ 60 rpm as it is illustrated in Figs. 5 and 6 in both transient and steady cases. This is due to the balance between inertial and viscous forces.

For low rotation speeds the viscous forces are dominant leading to a symmetric laminar flow regime whereas for high crystal rotation speeds the inertial forces are more significant

and the flow loses its symmetry.

### *4.2 Radial profile of temperature*

Fig 7 shows the radial profile of the temperature in case of steady state regime just under the melt- crystal interface z=0.098 m. These profiles presented for various rotation speeds, this confirms the results discussed earlier: $\omega_{cry} \leq 40$ rpm symmetry of temperature profile. $40 \leq \omega_{cry} \leq 50$ rpm The symmetry starts to disappear. For $\omega_{cry} \geq 60$ rpm, the flow becomes totally non-symmetric.

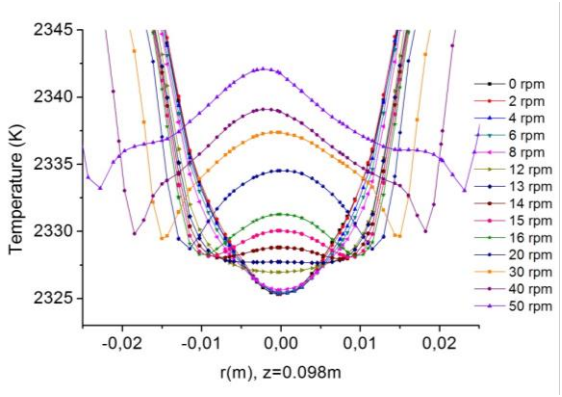


**Figure 7:** Radial profile of temperature just below the melt free surface (2 mm)

### *4.3 Optimal rotation speed*

The shape of the melt-crystal interface in the case of sapphire greatly related to the crystal rotation speed [Hans, Scheel and Capper (2008)]. This rotation speed plays an important role for influencing the shape of the interface during the Cz process [Tavakoli and Wilke (2007)]. In this part we have studied the shape of the crystal melt interface for a whole range of rotation speeds inside the interval where the flow is symmetric. Our objective is to find the optimal rotation speed leading to a flat crystal/melt interface. We have explored different rotation speeds up to 16 rpm. Fig. 8 shows the radial distribution of the temperature in the central region near the axis at the same horizontal plane 2 mm below the interface.

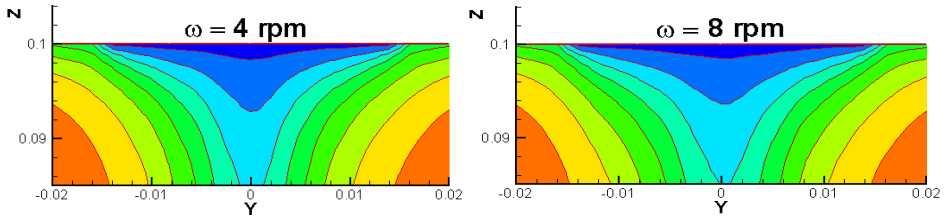

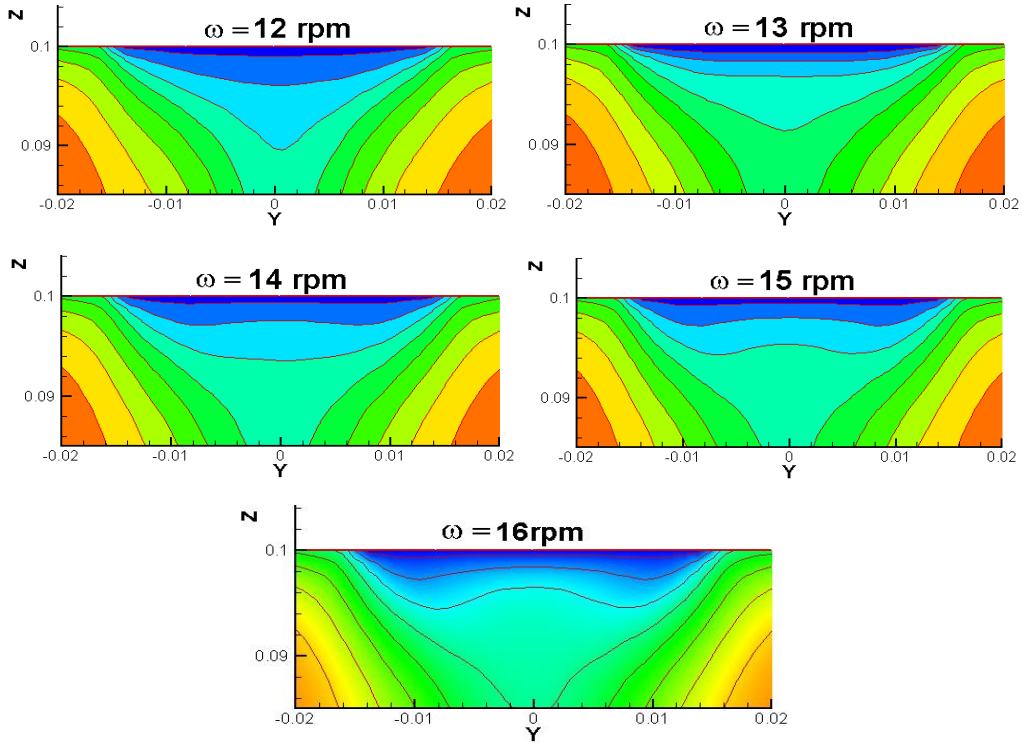


**Figure 8:** Isotherms of temperature showing the shape of melt-crystal interface formed by various rotation speeds

We notice that for relatively small rotation speeds $\omega_{cry} < 13$ rpm the shape of the melt-crystal interface is concave. For average rotation speeds $\omega_{cry} > 13$ rpm the shape of the interface is convex. For the rotation speed $\omega_{cry} = 13\,rpm$ the shape of the melt-crystal interface is flat. We can say that this rotation speed 13 rpm is an optimal speed which gives us a flat interface where the forced convection equals free convection. In this case we have obtained a good quality pulled crystal. Figure below confirms this result since the radial profile of temperature is flat for rotation speed $\omega_{cry} = 13$ rpm that is presented by the green color.

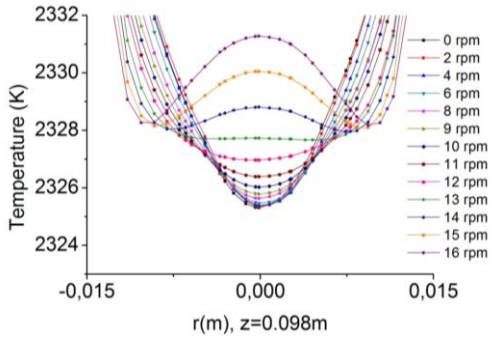


**Figure 9:** Radial profile of temperature for different rotation speeds

### *4.4 Thermal instabilities*

In order to study the thermal instabilities below the melt/crystal interface, we have performed the refined grid presented in Fig. 3. Temperature fluctuations near this interface are analyzed for different proposed rotation speeds using Fast Fourier Transform. These calculations were conducted under the melt/crystal interface taking into account the radiative heat transfer and Marangoni convection at the sapphire free surface melt.

#### *4.4.1 Analysis of temperature fluctuations*

We need to choose various points below the melt-crystal interface to better locate the position which having large temperature fluctuations. Five points were selected at a plan 2 mm (that is z=0.098 m) just below the melt-crystal interface: P0(0, 0, 0.098), P1(0.015, 0, 0.098), P2(0, 0.015, 0.098), P3(-0.015, 0, 0.098), P4(0, -0.015, 0.098). Fig. 9 shows the temperature fluctuation magnitude as a function of the frequency at these five chosen points.

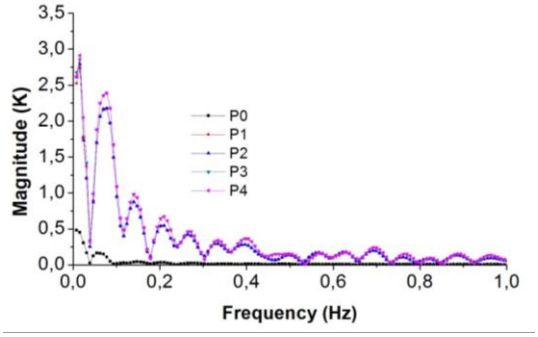


**Figure 10:** Temperature fluctuations spectra at various positions under the melt-crystal interface

According to this figure, for the point P4(0, -0.015, 0.098) the amplitudes of fluctuations is higher than those found for the other points. So P4 is the adopted point for our analysis.

#### *4.4.2 Time variation of the temperature*

Fig. 11 shows the time variation of the temperature for different crystal rotation speeds at the position P4 having larger fluctuations. The temperature asymptotic value is reached in about 200 s. This transient time is the same for all speeds lower than 20 rpm. The asymptotic value increases with $\omega_{cry}$ gradually for rotations speeds in the range $20 \text{ rpm} < \omega_{cry} < 30 \text{ rpm}$ reaching a limit value.

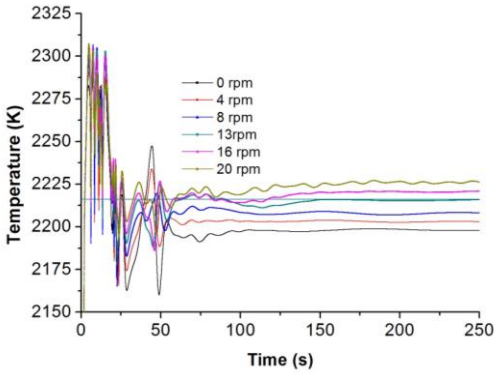


**Figure 11:** Time variation of the temperature at various crystal rotation speeds at the position P4

It is clear that the forced convection due to the crystal rotation enhances the heat transfer inside the melt, which increases the asymptotic value of the temperature after the transient regime. For relatively high rotation speeds, $\omega_{cry} \geq 40$ rpm the temperature becomes instable as shown in Fig. 12.

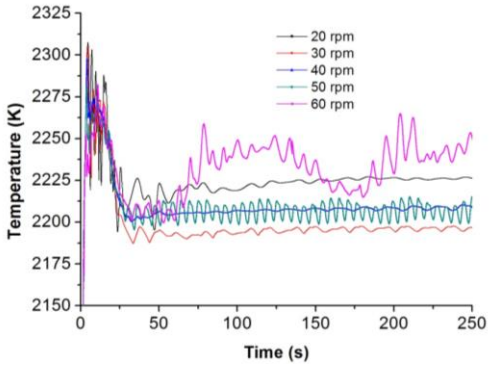


**Figure 12:** Time variation of the temperature at higher crystal rotation speeds

From Fig. 12, we notice that the temperature spectra are continuous and higher temperature magnitudes are observed for low frequencies. This is true for all rotation speeds. Furthermore, the temperature oscillations depend on the considered crystal speed and they are more important for the higher speeds than for the lower ones. That is for low rotation speeds the magnitude of the temperature is smaller.

*4.4.3 Temperature fluctuations*

We have also conducted an analysis of the temperature fluctuations just near this interface for different proposed rotation speeds using Fast Fourier Transform (FFT).

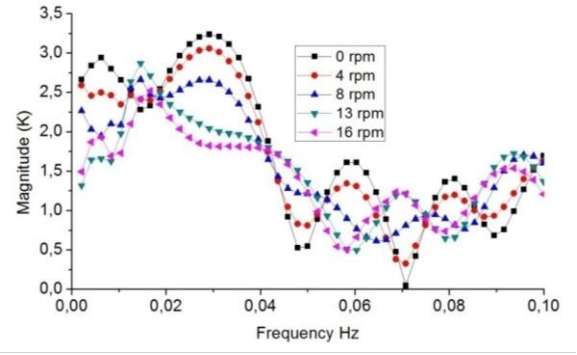


**Figure 13:** Fast Fourier Transforms of the temperature fluctuations at P4 (2 mm below the melt-crystal interface) for smaller crystal rotation speeds

The Magnitude spectrum does not depend on the crystal rotation speed in a simple way. Nevertheless we notice from Fig. 13, that the amplitude of the lower frequency mode (around 0.03 Hz) decreases when the rotation speed increases from 0 to 16 rpm. For rotation speeds higher than 20 rpm the spectra becomes instable with fluctuations and it becomes harder to analyse as shown in Fig. 14.

Since thermal fluctuations are detrimental to the quality of the grown crystal we conclude that the rotation speed has to be lower than 20 rpm in order to reduce the temperature fluctuations.

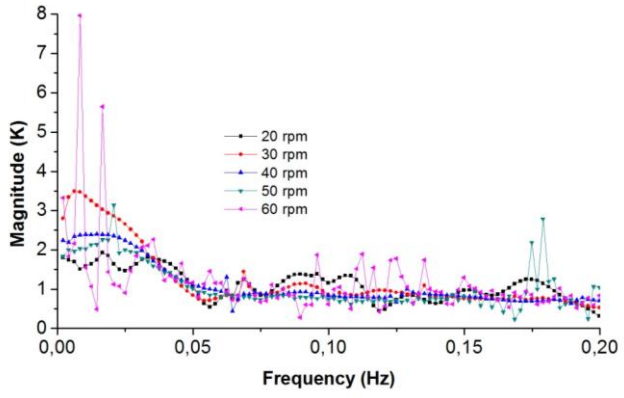


**Figure14:** Temperature fluctuations at for higher crystal rotation speeds

## 5 Conclusions

We have performed a three-dimensional numerical analysis of the crystal growth of sapphire using the Cz growth technique. Our aim is to improve the optimal conditions for growing efficiently high quality sapphire crystals with good thermal and optical properties. We have analysed thermal fluctuations near the melt-crystal interface and the convective heat transfer under the Czochralski process and presented a detailed investigation on the effects of the rotation speed and the temperature distribution on the crystal/melt interface shape under forced convection.

- We have been able to determine the optimal rotation speed giving a planar crystal-melt interface where the symmetry of the flow in the crucible is conserved. This occurs when a balance between inertial and viscous forces is realized.
- For low rotation speeds the viscous forces are dominant leading to a symmetric laminar flow regime whereas for high crystal rotation speeds the inertial forces are more significant and the flow loses its symmetry.
- The balance between inertial and viscous forces is necessary for the stability of the growing process of sapphire and gives good quality pulled crystals.
- The temperature spectrum is found to be continuous and higher temperature magnitudes are observed for low frequencies.
- The temperature magnitude is more important for higher speeds in a way that higher crystal rotation reduces the temperature fluctuations. Indeed the amplitude of the lower frequency mode decreases when the rotation speed increases.
- For relatively high rotation speeds $\omega_{cry} > 40$ rpm we notice a loss of flow symmetry in the crucible and a reduction of the axial speed which is translated by the birth of a radial and tangential movement and for $\omega_{\mathrm{cry}} \geq 60$ rpm the flow becomes totally three-dimensional.

**References**

**Alombert-Goget, G.; Li, H.; Guyot, Y.; Brenier, A.; Lebbou, K.** (2016): Luminescence and coloration of undoped and Ti-doped sapphire crystals grown by Czochralski technique. *Journal of Luminescence*, vol. 169, pp. 516-519.

**Azoui, H.; Laidoune, A.; Haddad, D.; Bahloul, D.; Merrouchi, F.** (2016): Numerical simulation of the crystal growth of Ti: $Al_2O_3$ material by the μ-PD Technology. *Journal of New Technology and Materials*, vol. 6, no. 2, pp. 102-110.

**Brandle, C.** (1982): Flow transitions in Czochralski oxide melts. *Journal of Crystal Growth*, vol. 57, no. 1, pp. 65-70.

**Bruni, F. J.** (2013): Will Czochralski growth of sapphire once again prevail. *Acta Physica Polonica A*, vol. 124.

**Chandra, P. K; Schmid, F.** (2001): Growth of the world's largest sapphire crystals. *Journal of Crystal Growth*, vol. 225.

**Derby, J.; Atherton, L.; Gresho, P. (**1989): An integrated process model for the growth of oxide crystals by the Czochralski method. *Journal of crystal growth*, vol. 97, no. 3, pp. 792-826.

**Duffar, T.** (2010): *Crystal growth processes based on capillarity: Czochralski, floating zone, shaping and crucible techniques*. John Wiley & Sons Ltd.

**Fukuda, T.** (2007): Shaped crystals, growth by micro-pulling-down technique. *Advances in Materials Research*, vol. 8.

**Gałazka, Z.; Wilke, H.** (2000): Influence of marangoni convection on the flow pattern in the melt during growth of Y3AI5O12 single crystals by the Czochralski method. *Journal of Crystal Growth*, vol. 216, no. 1, pp. 389-398.

**Hans, J. S.; Capper, P.** (2008): *Crystal Growth Technology*. Wiley-VCH Verlag GmbH & Co. KGaA, Weinheim.

**Jing, C.; Imaishi, N.; Sato, T.; Miyazawa**, **Y.** (2000): Three-dimensional numerical simulation of oxide melt flow in Czochralski configuration. *Journal of Crystal Growth*, vol. 216, no. 1, pp. 372-388.

**Kimura, H.** (1986a): Flow transitions in simulated Czochralski method with tetradecane instead of $bi_{12}siO_{20}$. *Journal of crystal growth*, vol. 78, no. 1, pp. 19-23.

**Kimura, H.** (1986b): Growth instability in simulations of the Czochralski method with tetradecane and water. *Journal of Crystal Growth*, vol. 78, no. 2, pp. 322-324.

**Kobayashi, N.** (1978): Computational simulation of the melt flow during Czochralski growth. *Journal of Crystal Growth*, vol. 43, no. 3, pp. 357-363.

**Laidoune, A.** (2010): *Croissance des fibres cristallines pour usage dans l'optoélectronique (Ph.D Thesis)*. University of Batna1-Batna, Algeria.

**Nehari, A.** (2011): *Etude et caractérisation de la synthèse de milli-billes d'alumine alpha et de la cristallogenèse du saphir pur et dopé titane ($Ti^{3+}$) (Ph.D Thesis)*. University of Lyon, France.

**Nguyen, T. P.; Hsieh, Y. T.; Chen, G. C.; Hu, C.; Nguyen, B. H.** (2016): Effect of crucible and crystal rotations on the convexity and the thermal stress in large size sapphire crystals during Czochralski growth. *Journal of Crystal Growth*, vol. 468, pp. 514-525.

**Rahal, S.; Cerisier, P.; Azuma, H.** (2008): Application of the proper orthogonal decomposition to turbulent convective flows in a simulated Czochralski system. *International Journal of Heat and Mass Transfer*, vol. 51, pp. 4216-4227.

**Soltani, N.; Rahal, S.** (2017): Control of the convective flow instabilities in a simulated Czochralski growth system. *Fluid Dynamics & Materials Processing*, vol. 13, no.1, pp. 1-17.

**Stelian. C.; Nehari, A.; Lasloudji, I.; Lebbou, K.; Dumortier, M. et al.** (2017): Modeling the effect of crystal and crucible rotation on the interface shape in Czochralski growth of piezoelectric langatate crystals. *Journal of Crystal Growth*, vol. 475, pp. 368-377.

**Tavakoli, M. H.** (2008): Numerical study of heat transport and fluid flow during different stages of sapphire Czochralski crystal growth. *Journal of Crystal Growth*, vol. 310, pp. 3107-3112.

**Tavakoli, M. H.** (2014): Computational study of convective and radiative heat transport in Czochralski growth of oxides. *Sop Transactions on Applied Physics*, vol. 1, no. 2.

**Tavakoli, M.; Wilke, H.** (2007): Numerical investigation of heat transport and fluid flow during the seeding process of oxide Czochralski crystal growth part 2: Rotating seed. *Crystal Research and Technology*, vol. 42, no. 7, pp. 688-698.

**Tavakoli, M.; Wilke, H.; Crnogorac, N.** (2007): Influence of the crucible bottom shape on the heat transport and fluid flow during the seeding process of oxide Czochralski crystal growth. *Crystal Research and Technology*, vol. 42, no. 12, pp. 1252-1258.

**Wu, X. B.; Geng, X.; Guo, Z. Y.** (1996): Fundamental study of crystal/melt interface shape change in Czochralski crystal growth. *Journal of Crystal Growth*, vol. 169, no. 4, pp. 786-794.

**Xiao, Q.; Derby, J. J.** (1995): Three-dimensional melt flows in Czochralski oxide growth: High-resolution massively parallel, finite element computations. *Journal of Crystal Growth*, vol. 152, no. 3, pp. 169-181.

**Xiao, Q.; Derby, J. J.** (1994): Heat transfer and interface inversion during the Czochralski growth of yttrium aluminum garnet and gadolinium gallium garnet. *Journal of Crystal Growth*, vol. 139, no. 1-2, pp. 147-157.

**Yan, Z.; Shalapska, T.; Bourret, E. D.** (2016): Czochralski growth of the mixed halides BaBrCl and BaBrCl: Eu. *Journal of Crystal Growth*, vol. 435, pp. 42-45.